ARL-TR-10350 ● MAY 2026

In Situ Tracking of Phase Changes Within an Additively Manufactured Steel via Laser Ultrasound

by Frank Kellogg, Michael Rupinen, Alexender Butler, Andelle Kudzal, Joshua Taggart-Scarff, and Daniel Field

NOTICES

Disclaimers

The research in this report was performed in connection with contract/instrument W15P7T-19-D-0126 with the U.S. Army Combat Capabilities Development Command (DEVCOM) Army Research Laboratory (ARL).

The findings in this report are not to be construed as an official Department of the Army position unless so designated by other authorized documents. The views and conclusions contained in this document are those of SURVICE Engineering and ARL.

Citation of manufacturer's or trade names does not constitute an official endorsement or approval of the use thereof.

Destroy this report when it is no longer needed. Do not return it to the originator.

ARL-TR-10350 ● MAY 2026

In Situ Tracking of Phase Changes Within an Additively Manufactured Steel via Laser Ultrasound

Frank Kellogg
SURVICE Engineering

Michael Rupinen, Alexander Butler, Joshua Taggart-Scarff, and Daniel Field
DEVCOM Army Research Laboratory

Andelle Kudzal
Air Force Research Laboratory

REPORT DOCUMENTATION PAGE

1. REPORT DATE	2. REPORT TYPE	3. DATES COVERED	
		START DATE	END DATE
May 2026	Technical Report	3/24/2025	11/28/2025

4. TITLE AND SUBTITLE
In Situ Tracking of Phase Changes Within an Additively Manufactured Steel via Laser Ultrasound

5a. CONTRACT NUMBER	5b. GRANT NUMBER	5c. PROGRAM ELEMENT NUMBER
5d. PROJECT NUMBER	**5e. TASK NUMBER**	**5f. WORK UNIT NUMBER**

6. AUTHOR(S)
Frank Kellogg, Michael Rupinen, Alexander Butler, Andelle Kudzal, Joshua Taggart-Scarff, and Daniel Field

7. PERFORMING ORGANIZATION NAME(S) AND ADDRESS(ES)
DEVCOM Army Research Laboratory
ATTN: FCDD-RLA-MD
Aberdeen Proving Ground, MD 21005

8. PERFORMING ORGANIZATION REPORT NUMBER
ARL-TR-10350

9. SPONSORING/MONITORING AGENCY NAME(S) AND ADDRESS(ES)	10. SPONSOR/MONITOR'S ACRONYM(S)	11. SPONSOR/MONITOR'S REPORT NUMBER(S)

12. DISTRIBUTION/AVAILABILITY STATEMENT
DISTRIBUTION STATEMENT A. Approved for public release: distribution unlimited.

13. SUPPLEMENTARY NOTES
ORCIDs: Frank Kellogg, 0000-0003-3048-0255; Michael Rupinen, 0009-0009-9438-9902; Alexander Butler, 0009-0002-3705-4961; Andelle Kudzal, 0000-0001-8762-8228; Joshua Taggart-Scarff, 0000-0003-3540-7436; Daniel Field, 0000-0002-8890-4391

14. ABSTRACT
Metals-based laser powder bed fusion (LPBF) additive manufacturing (AM) involves the rapid melting, solidification, and reheating of metallic powder as parts are built layer-by-layer. This process can lead to the development of residual stress within the part, which can be large enough to cause the sample to tear itself apart when being removed from the build plate, creating the need for stress-reducing heat treatments after each build. In this study, microstructural changes to a low-alloy, high-strength steel produced via LPBF were monitored in situ during simulated low-temperature stress reliefs using a Laser Ultrasound Measurement (LUMet) add-on to a Gleeble 3800 system. Ultrasound techniques are influenced by several factors including stress state, microstructure, and temperature; thus, LUMet testing was complemented with X-ray diffraction, dilatometry, and microscopy to further elucidate the mechanisms leading to changes in signals. Based on the combined results, it appears that the LUMet can track the decomposition of retained austinite in the LPBF AM samples during stress-relief simulations on the Gleeble.

15. SUBJECT TERMS
Terminal Effects, Sciences of Extreme Materials, in situ measurements, additively manufactured steel, laser ultrasound, Gleeble testing, austinite decomposition

16. SECURITY CLASSIFICATION OF:			17. LIMITATION OF ABSTRACT	18. NUMBER OF PAGES
a. REPORT	b. ABSTRACT	C. THIS PAGE		
UNCLASSIFIED	UNCLASSIFIED	UNCLASSIFIED	UU	28

19a. NAME OF RESPONSIBLE PERSON	19b. PHONE NUMBER *(Include area code)*
Frank Kellogg	(520) 691-5862

STANDARD FORM 298 (REV. 5/2020)
Prescribed by ANSI Std. Z39.18

Contents

List of Figures

List of Tables

1. Introduction

Laser powder bed fusion (LPBF) additive manufacturing (AM) is the process of building parts through the rapid melting and solidification of thin layers of metallic powders.[1] The repetition of the rapid melting and solidification process can lead to the buildup of residual stresses, which can then lead to part failure during the build process or part removal from the build plate, creating the need for postbuild stress-relieving heat treatments. Stress-relief heat treatments designed for AM parts can be difficult to develop, especially in cases where a designed microstructure needs to be maintained. They can be determined by applying a matrix of temperature–time combinations to subsequent build plates and measuring some property (deflection, tensile ductility, Charpy v-notch [CVN] impact energy, etc.) to determine the optimal heat treatment as a balance between part survivability and property retention.[2–4] This approach requires a large number of samples and long build times. An in situ approach that could show clear signals *during* heating may allow for rapid optimization of stress-relief treatments and increased understanding of mechanistic changes with heat treatment.

In addition to significant residual stress, AM martensitic steels often have large fractions of retained austenite present relative to what would be expected in the conventionally fabricated condition of the steel.[2–4] This retained austenite may significantly affect the properties of the steel, particularly CVN toughness. Thermal treatments such as stress-relief treatments may lead to decomposition of some of the retained austenite; therefore, an understanding of austenite decomposition with stress-relief treatments is also of significant interest and value to the process designer.

In situ investigations into microstructure evolution with heating may be performed using several techniques[5] including dilatometry, neutron, high-energy X-ray diffraction (XRD), and laser ultrasound. For this work, laser ultrasound in conjunction with dilatometry was chosen because of its ability to heat and measure samples in situ in a Gleeble3800 using the Laser Ultrasound Measurement (LUMet) add-on* for use with Gleeble systems.

The basis behind ultrasound techniques is that, for a given material at a given temperature, the speed of sound (SS) through the material is a constant; any changes to the microstructure changes the SS through the material. The basis for laser ultrasound generation dictates that when a laser strikes a sample, surface heat is generated that leads to volume expansion. This constrained volume change creates ultrasonic pressure waves that travel through the material, the echoes of which can

* Developed by Tecnar and licensed to Dynamic Systems Inc.

be measured to calculate the SS through the sample. This theory is the basis for using ultrasound measurements to monitor changes within a material—whether cracks from in-service usage or microstructural changes such as grain growth, precipitate formation, phase change, etc.[6–15] While using ultrasound to evaluate part integrity and calculate elastic properties at room temperature (RT) is well established[3]; using ultrasound to investigate microstructural features, especially at non-ambient temperature, is not nearly as common.[6–15] The LUMet add-on for use with Gleeble systems is one of the only commercial items available that can reportedly use ultrasound measurements in situ to determine microstructural behavior at temperature.[13–15] In this study, the LUMet was used to track changes in the SS during heat treatments to stress-relieve high-strength, low-alloy AM built steel samples. The LUMet measurements were complemented with dilatometry, XRD, and mechanical testing to correlate changes in the LUMet signal to changes in microstructure and properties. The experiments were designed to determine if the LUMet system could detect differences among applied stress-relief treatments and to determine which microstructural changes the system was tracking.

2. Methods

2.1 Stress-Relief Heat Treatment Study

Prior to initial LUMet testing, a detailed experiment on the effect of stress-relief temperature on mechanical properties was conducted. A total of 30 CVN samples (notched during postprocessing) and 30 subscale tensile bars[16] were made from a low-alloy, high-strength steel via LPBF AM using a Renishaw 400 system with in-house optimized build parameters.[17] Sets of five samples were then subjected to one of six possible stress-relief heat treatments (Table 1). These experiments were used to determine if shorter heat treatment times/temperatures could replace the higher-temperature, more-complicated schedules previously published.[3] Tensile samples were pulled along the build direction (at a strain rate of 1 mm/min), while the CVN samples were notched perpendicular to the build direction and tested according to the ASTM E23 standard[18] for impact testing at RT. The study's findings were then used to determine in situ test ranges for the LUMet testing.

Table 1. Stress-relief heat treatment cycles.

Temperature (°C)	Hold time (h)	Cooling method
200	2	Furnace cool
300	2	Furnace cool
400	2	Furnace cool
500	2	Furnace cool
600	2	Furnace cool
No stress relief		

2.2 LUMet Trials

Based on the results from the initial stress-relief study, the temperature range from 200 to 300 °C was identified as the primary range of interest for stress relief due to the mechanical properties obtained. Using the established build parameters[14] parts were printed in the specified LUMet test geometry (Figure 1A). Samples were made during two different runs: samples from one run were stress-relieved (SR) at 200 °C for 2 h, and samples from the other run were not stress-relieved (NSR) to determine if the in situ monitoring could differentiate between the two sample conditions. Dog bone samples (Figure 1B) were also made to investigate whether in situ monitoring could differentiate between strained samples (i.e., samples that were loaded in tension to predetermined strains and then had LUMet samples machined out of their gauge sections). Samples were removed from the build plate via electrical discharge machining and were then subjected to low force grinding to remove the overly rough surfaces characteristic of AM processing and ensure parallelism of the surfaces.

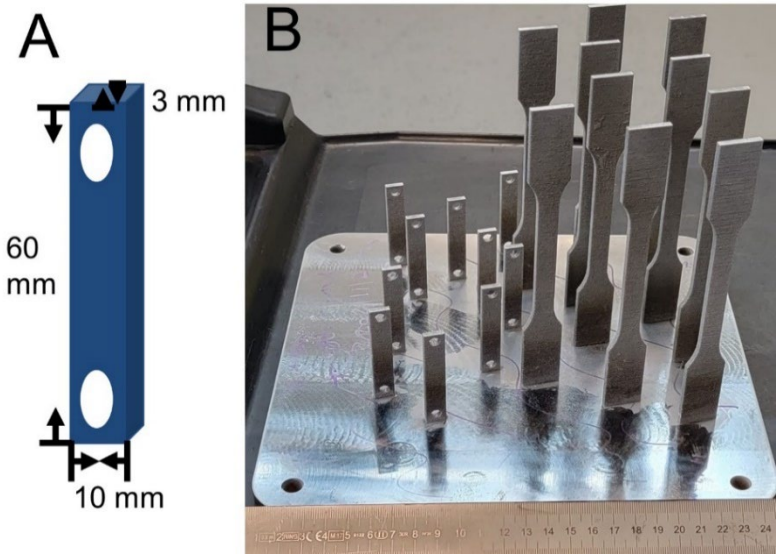

Figure 1. A) Schematic showing LUMet sample and B) samples after printing.

Samples for LUMet testing had k-type thermocouple leads welded at the center of the sample and were then loaded into the Gleeble3800 system (running the pocket jaw mobile conversion unit). The LUMet add-on was installed and set up in the back of the Gleeble tank (Figure 2). The Gleeble testing chamber/tank was evacuated to a pressure/vacuum level in the range of 10^{-5} to 10^{-6} torr.

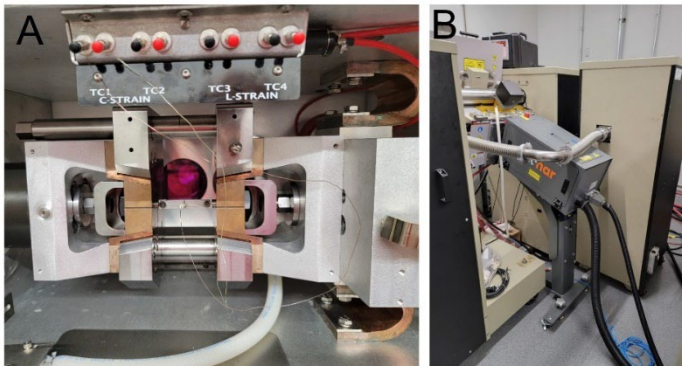

Figure 2. A) LUMet sample loaded into the Gleeble and B) laser mounted to the back of the Gleeble.

Tested thermal cycles for simulating stress relief are presented in Table 2. During heating, the measured RT was between 17 °C (at the start of experiments) and 30 °C (at the end of experiments). Samples were heated at 10 °C/s and cooled by turning off the resistive heating; samples were allowed to cool in the chamber under vacuum. During heating, the Gleeble was programmed to maintain a load of 0 kgf to allow for thermal expansion. For the LUMet study, peak temperatures of either 200 or 300 °C were chosen to simulate the original stress relief for the NSR samples and to determine the effect of a higher stress relief temperature on the SR and NSR samples.

Table 2. Stress-relief simulation thermal cycles.

Temperature (°C)	Time at each temperature (min)	Total experimental time (min)	SR	NSR	Prestrained (0.02, 0.05, 0.08 strain) (SR)
RT-200-RT	20	60	×	×	. . .
200-300-200	20	60	×	. . .	. . .
RT-200-300-200-RT	15	75	×	×	×
RT-300-RT: one heating cycle	20	20	. . .	×	. . .
RT-300-RT: four heating cycles	2 (at 300)	49.76	. . .	×	. . .
RT-300-RT: five heating cycles	2 (at 300)	64.76	. . .	×	. . .

The LUMet is a two-laser unit where one laser is used to generate shock waves within the sample (the generation laser) while the detection laser (second laser) is

used to measure the shock waves as they echo back and forth within the sample (Figure 3).

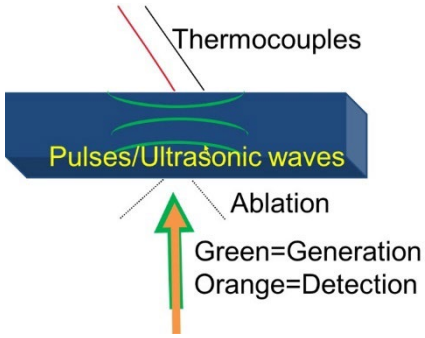

Figure 3. Diagram of laser sound generation in a Gleeble sample.

As the generation laser on the LUMet is a class 4 laser, it can, and does, ablate the sample during testing. Experiment times were chosen to try and balance overall exposure time to the sample, laser sampling rate, and time needed to obtain enough waveforms for proper analysis addressing the ablation effect (data quality decreases rapidly as sample ablation increases).

2.3 Characterization Methods

After heat-treatment simulation, the samples were cut and prepared for XRD and hardness testing. Samples were ground to 1200 grit and analyzed using a Bruker D2 Phaser XRD unit with a cobalt source. Phase fractions were determined using Rietveld refinement. Following XRD analysis, hardness was measured using Rockwell C indents. In both cases, measurements were made in the lateral position as the LUMet measurements but on the opposite side of the sample. In addition to the sample conditions in Table 1, additional samples were examined via XRD and subjected to hardness testing, including samples in the as-printed, as-SR, heated to and held at 200 °C for 60 min (SR-condition only), and heated to and held at 300 °C for 60 min (SR-condition only) conditions.

Select samples were prepared for electron microscopy and polished to 0.25-µm diamond finish followed by a 4-h vibratory polish in 0.02-µm colloidal silica. Electron backscatter diffraction (EBSD) was performed using a 20 kV accelerating voltage and 6.4-µA beam current on a Tescan scanning electron microscope. Samples were then etched using a 4% nital solution and imaged using secondary electrons to examine the bulk microstructure.

As another way to verify what changes in the LUMet signal might indicate, several of the thermal runs (i.e., the RT-200 °C loop, the RT-200-300 °C loop, and the RT-300 °C loop for one, four, and five cycles) using both SR and NSR samples were

replicated in a Linseis DIL L78 QDT/RITA dilatometer. Dilatometry specimens were machined to 4.0 × 1.5 × 10.0 mm. The same thermal profile used in the Gleeble experiments was programmed into the dilatometer.

3. Results and Discussion

3.1 Mechanical Testing of Stress-Relief Heat Treatments

Mechanical testing of SR samples at various temperatures was used to determine the optimum stress-relief temperature for eliminating cracking and generating the best combination of toughness and strength. Figure 4 shows the respective properties versus stress-relief temperature (samples tested at 25 °C were not SR). The hardness data (Rockwell C, measured from the base of the CVN samples after testing; Figure 4A) shows a general increase in hardness up to a stress-relief temperature of 500 °C with a significant drop in hardness following a 600 °C stress relief. When comparing the hardness data with the tensile data, there appears to be little correlation between yield strength or ultimate tensile strength (UTS) and hardness, which is somewhat surprising. Austenite and its stability can significantly influence the mechanical response of steel and could be one explanation for this observation. The strain to failure tensile data (Figure 4B) shows that the SR sample at 200 °C failed at a higher strain than any of the other samples while also having the second-highest yield and ultimate strengths (Figures 4C and 4D). The Charpy impact data (Figure 4E) also showed that the 200 °C stress relief led to the highest impact toughness but was close to the values measured for the SR samples at 300 and 400 °C (with a large drop in toughness at higher stress-relief temperatures). As the 200 °C condition displayed the best combination of strength and toughness/ductility, 200 °C was thought to be the optimal stress-relief temperature.

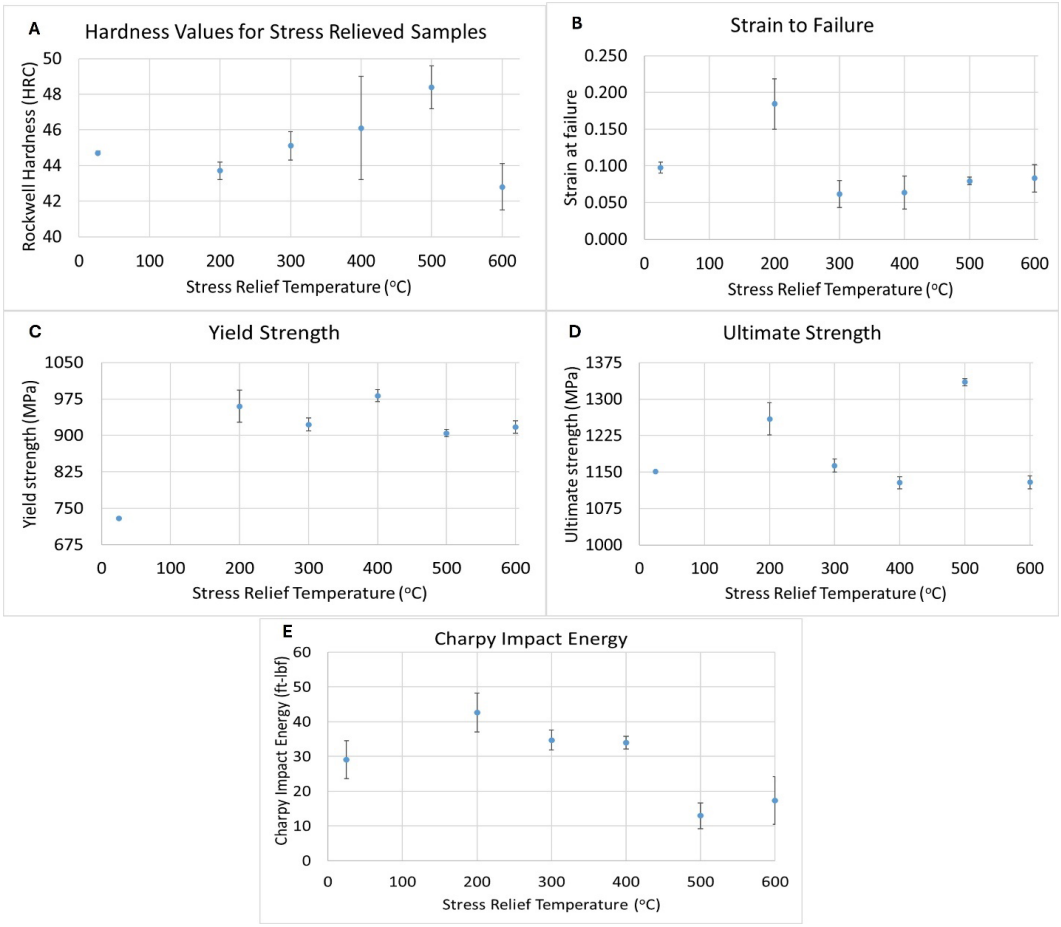

Figure 4. Mechanical test data from SR samples.

3.2 LUMet Results: SR Samples (200 °C, 2 h)

In general, the LUMet calculates the SS through a sample by measuring how long it takes for preselected echoes to be detected between consecutive waveforms. As a rule, and for these results, the second echo was chosen (i.e., the time between the second echo for waveform X and waveform X + 1). For this study, measurements of the SS were made at RT, 200/300 °C, and then again at RT for samples that were already SR at 200 °C for 2 h prior to LUMet testing (Figure 5). The 300 °C upper limit was chosen as it showed lower properties than the 200 °C conditions—particularly for the strain to failure and UTS—and it is traditionally associated with the tempered martensite embrittlement region in quenched and tempered steels. Figure 5 shows the change in the measured sound velocity over time for SR samples subjected to four different thermal cycles as a function of temperature and time. The differences in the starting velocity for each run are understood to be due to variation in sample thickness from different amounts of grinding needed to remove the surface roughness from the printing process as well as microstructural

differences due to texturing, the presence of multiple phases, and porosity. Despite these variations in thickness among samples, inferences may still be made from changes in the velocity within a single sample. Any changes in SS at RT at the end of the experiment relative to the start of the experiment were taken to mean that there were microstructural changes during the experiment. Figure 5A includes data from a sample held at RT with SS collected for 1 h to show that the laser by itself is not inducing any microstructural changes (despite ablating the test surface) as well as to show that, at least at RT, the damage from the laser is not enough to disrupt data collection. For each of the datasets in the graph (the various thermal loops) straight lines have been added to more easily demonstrate that there were changes with the RT SS values measured after heating the samples.

After the initial stress-relief run, heating to 200 °C for an additional 20 min is enough to generate changes in the RT LUMet measurements (Figure 5C), while heating to 300 °C leads to larger changes in measured SS not just at RT (Figure 5C) but also at 200 °C (Figure 5B). It is notable that the SS is higher for the second 200 °C hold for both loops reaching a max of 300 °C. The RT differences may be partially obscured by differences in the starting and ending chamber temperature. Another challenge when using an AM part is that the sampling location may move during the test. In a relatively homogeneous part, the exact placement of the laser may not be hugely significant; however, in a part with significant differences in porosity, texture, or thermal history (as seen in AM) these small moves may significantly affect the readings.

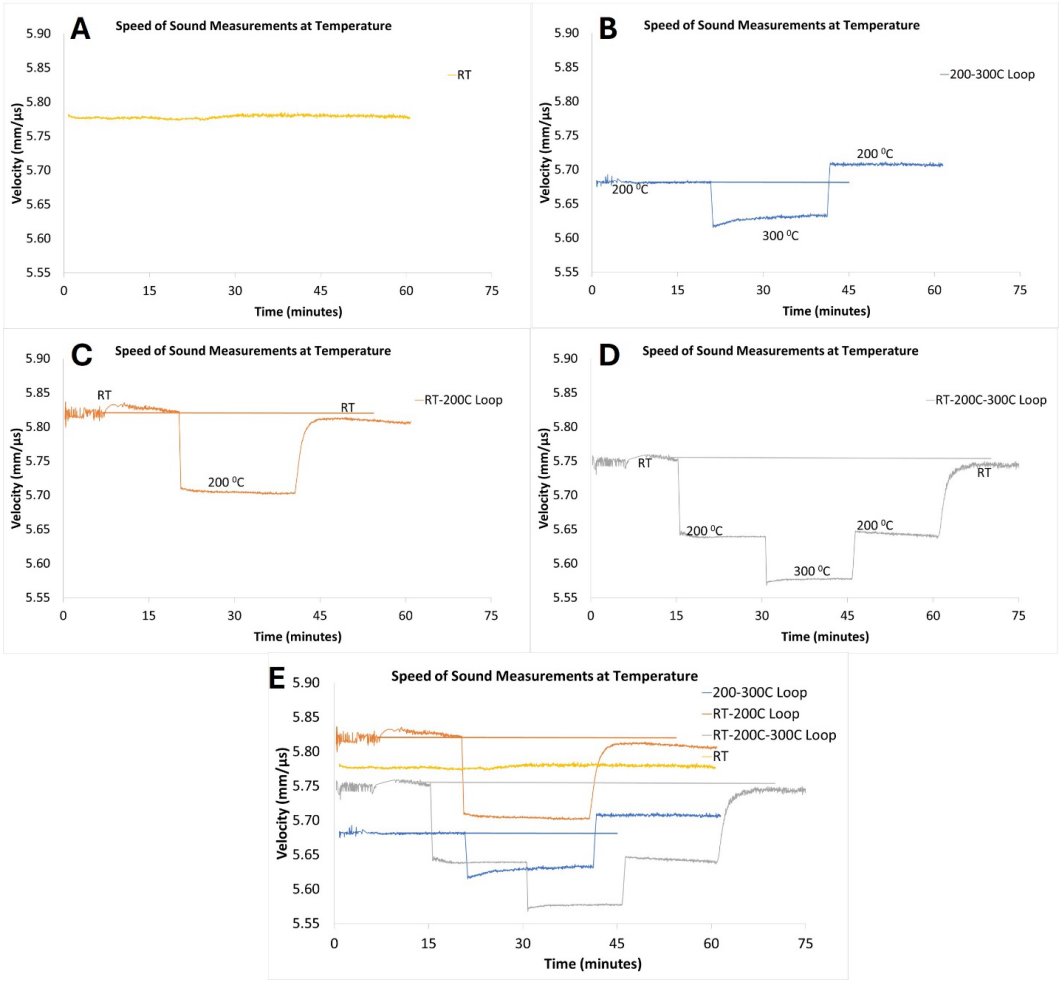

Figure 5. LUMet data for the SR samples cycled between RT, 200, and 300 °C.

3.3 LUMet Results: NSR Samples

The LUMet results for the NSR samples (Figure 6) had some significant differences from the SR samples.

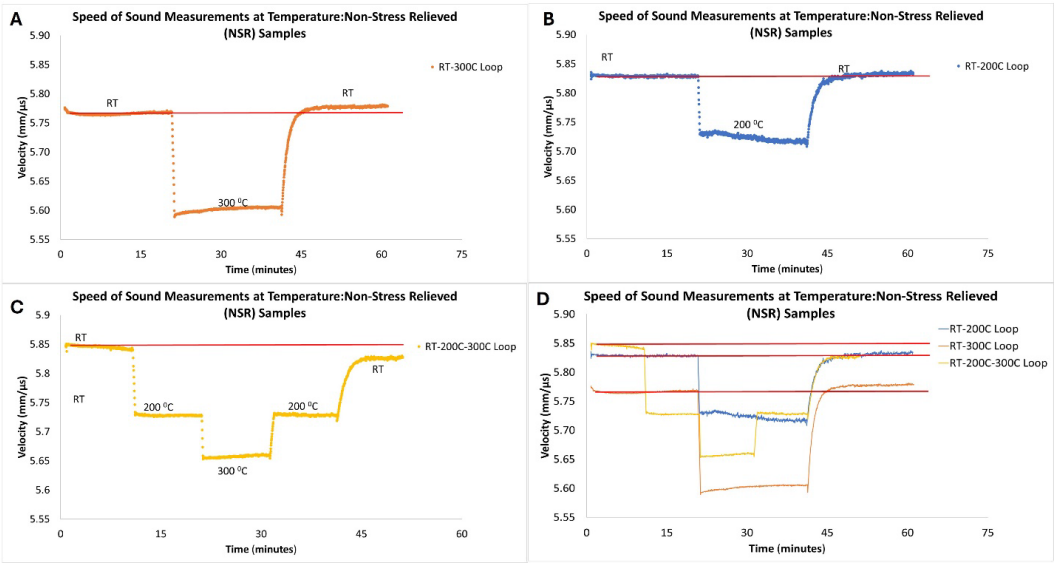

Figure 6. LUMet data for the NSR samples cycled between RT, 200, and 300 °C.

The most significant difference is that the RT- 200 °C loop sample did not have any changes in SS from beginning to end (Figure 6B). While the signal had a steady change during the 20-min hold at 200 °C the measured SS at RT after heating was the same as before heating. It is unclear if offsetting changes in microstructure occurred. However, both samples that were heated to 300 °C had SS changes at RT after heating (Figures 6A, 6C, and 6D). This provides some insight into the kinetics of the microstructural change seen in the SR sample. It is speculated that time is a critical component for the signal at 200 °C where the 2-h stress relief may lead to more marked microstructural changes compared with the shorter 20-min hold during the in situ experiment.

At 300 °C, changes in the SS are observed in both the SR and NSR states (Figures 5 and 6), indicating that at this temperature the microstructural change is more severe and produces a larger signal. This qualitatively correlates with the significant changes in mechanical properties shown in Figure 4. The possible microstructural features to consider are ferrite/martensite, carbides, and austenite, which affect the measured SS. Austenite should have the lowest SS with an increase in SS for martensite/ferrite and then tempered martensite.[19] Decomposition of austenite into martensite would tend to increase the SS in the sample while tempering of martensite/carbide formation would tend to decrease the SS in the sample relative to just a martensitic structure.

In Figures 7 and 8, samples without stress relief were thermally cycled between RT and 300 °C (10 °C/s heating, 2-min hold at 300 °C , and 10 min of cooling with a cooling rate of –0.25 °C/s to reach RT) to see how many cycles it would take before there were no longer any observed changes in the RT SS measurements (i.e., forcing the microstructural change to completion). One sample was subjected to four cycles (Figure 7) over a total experimental time of roughly 50 min and another to five cycles (Figure 8) over 63 min.

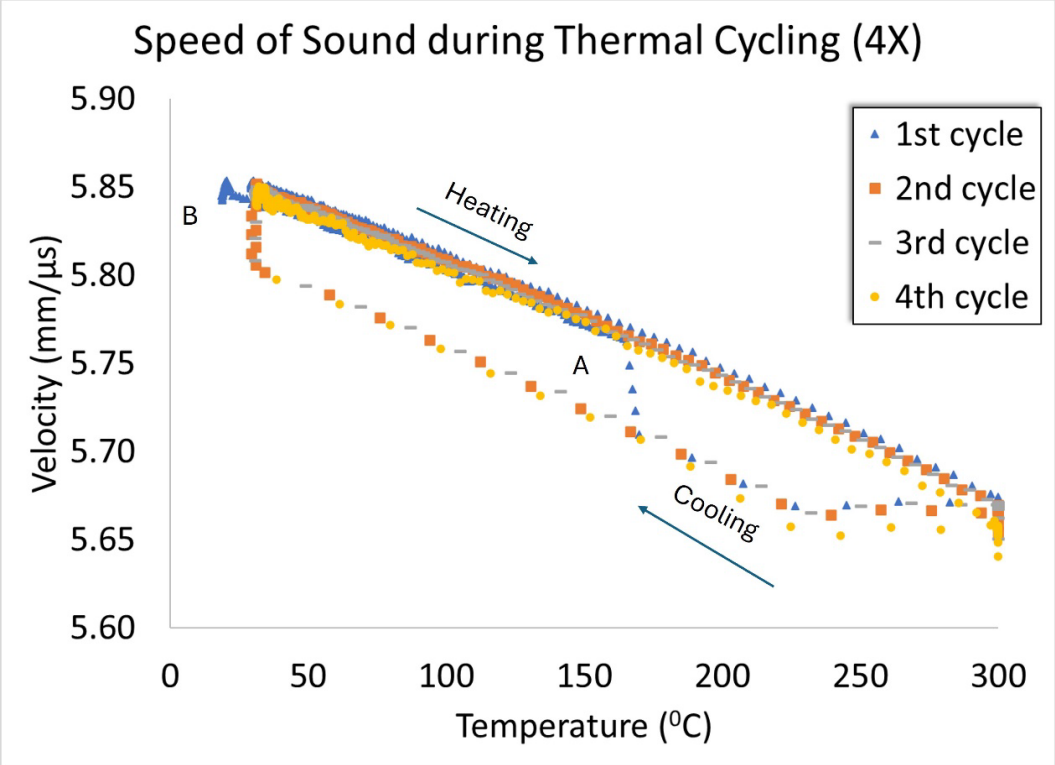

Figure 7. LUMet measurements during four heating cycles from RT to 300 °C on NSR sample.

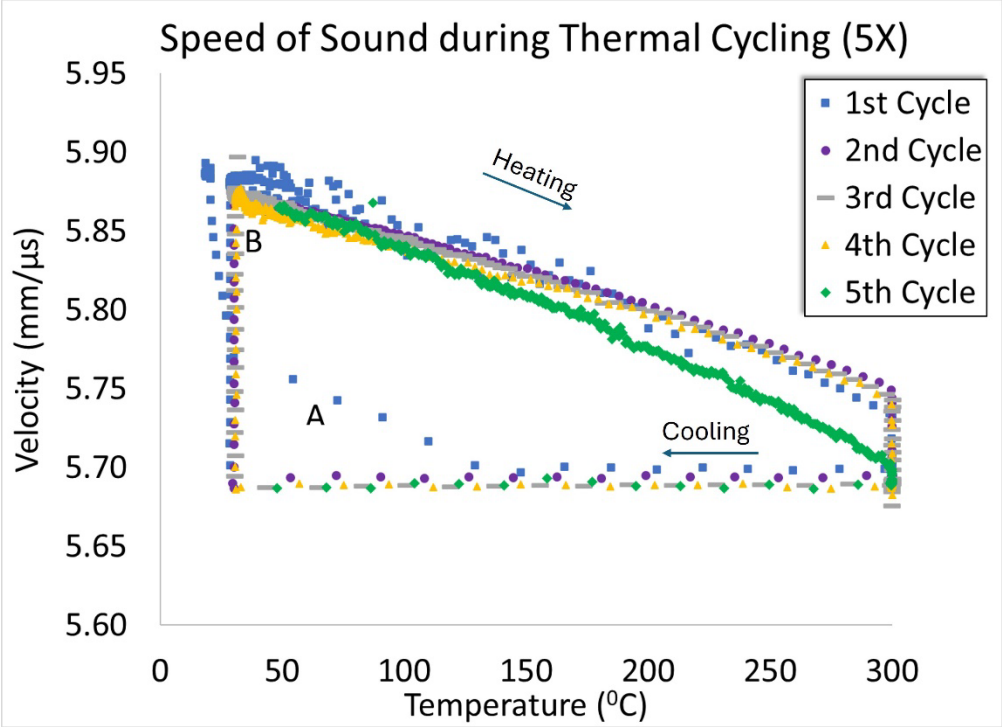

Figure 8. LUMet measurements during five heating cycles between RT and 300 °C on NSR sample.

The measured SS during the initial heating cycle changes as a function of increasing temperature differently than during any of the other cycles; there is a sharp decrease in the SS between 150 and 200 °C (Figures 7A and 8A) that is not replicated on subsequent cycles. It seems likely that this change in path is linked to changes to the sample surface due to ablation (as previously noted) rather than microstructural in nature. In the previous measurements (Figures 5 and 6) there is a long hold at RT to begin each measurement where the data is fairly noisy that might mask this effect; indication of this being an artifact is that it occurs at a temperature too low for microstructural changes in steel and after a very short period of time of approximately 17 s.

During the four cycles, the second and third cycles have essentially the same SS measurements while the fourth cycle is slightly different. When a sample was subjected to five cycles (Figure 8), the difference between the fifth cycle and the rest of the cycles was the largest difference observed, suggesting that it takes two to four cycles of heating to 300 °C before a significant volume of the microstructure changes. Previously, in a sample heated to 300 °C (NSR, Figure 6A), a small change in SS measurements at RT was observed, akin to the differences among cycle four and the first three in Figure 7 and the differences among cycles one and two through four in Figure 8.

3.4 LUMet Results: Prestrained Samples

One of the issues that quickly became apparent during these experiments is that laser ultrasound is not a good technique for making one-to-one sample comparisons. As seen in Figures 5E and 6D, when stacked together, the RT measurements of samples from the same material and build are noticeably different (this can be attributed to sample-to-sample variations due to texturing, phase volume differences, surface treatment differences, etc.). This meant that it was not possible to relate differences in the RT signal to different strain levels within the prestrained dog bone samples as there are no ways to differentiate signal differences due to thickness/surface condition from differences due to strain levels. It is still interesting to compare SS in the prestrained samples as it was anticipated that the strain could transform any retained austenite present in the steel,[4] which should also affect the SS. Dog bones were loaded in tension and pulled to strains of 0.02, 0.05, and 0.08 (samples pulled to failure failed at ~0.12 and ~0.15 strains, Figure 9).

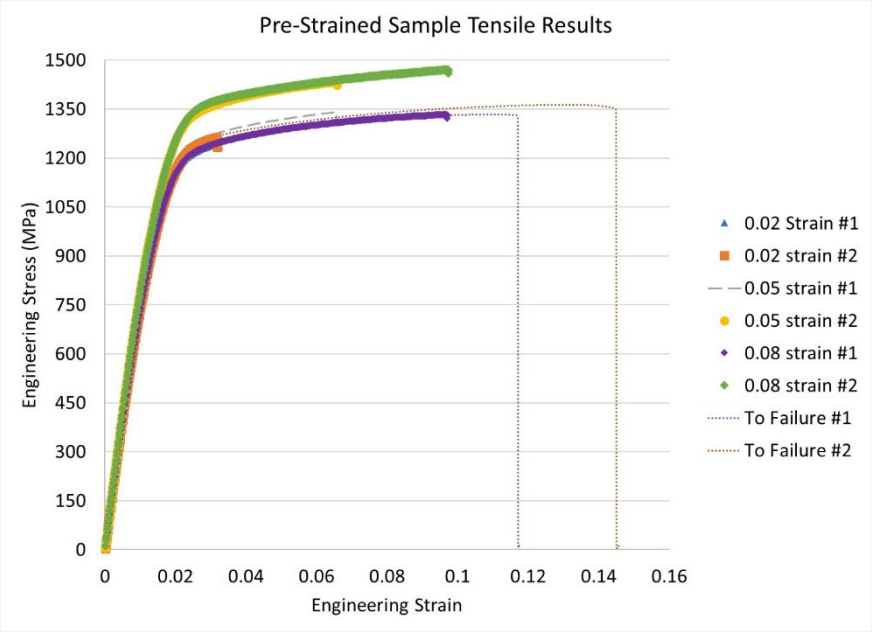

Figure 9. Prestrained sample tensile testing results.

The LUMet results for SR samples (Figure 10) that were prestrained to different amounts prior to LUMet testing are shown in Figure 10. In general, it would be expected that increased strain would lead to lower longitudinal SS; however, due to the starting material condition, comparing different samples is not necessarily meaningful. In general, it appears that all three samples end at a higher velocity than where they started. The greater starting velocity with greater initial strain is also noted but no explanation is clear at this time.

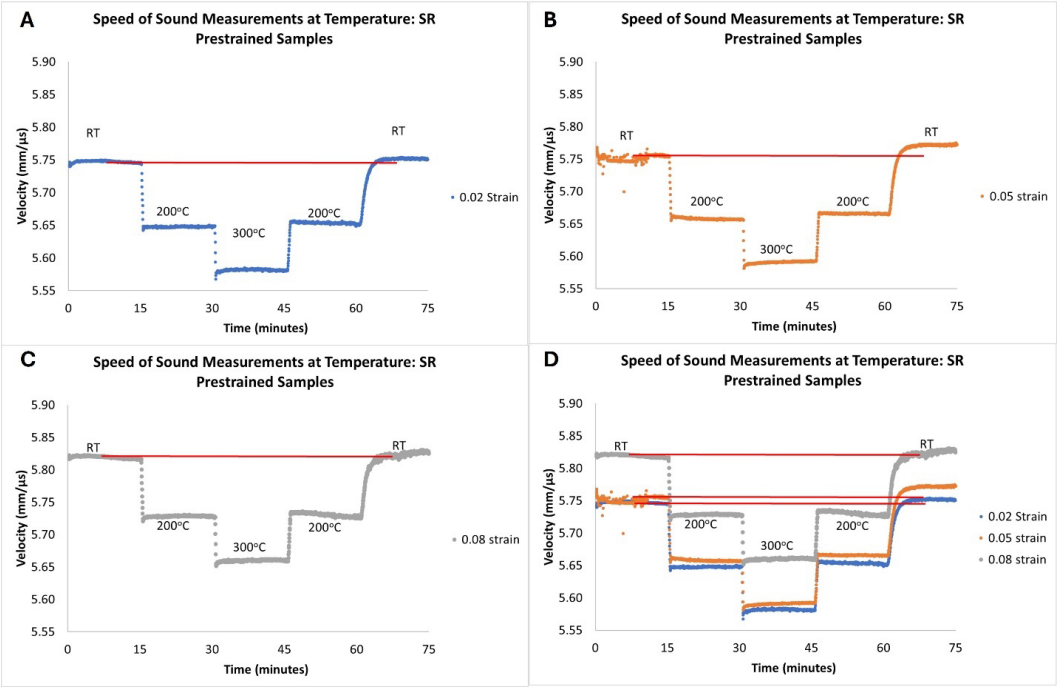

Figure 10. LUMet data for prestrained SR samples.

While some changes in signal were observed during the LUMet testing, it is necessary to determine the cause of the changes. A two-pronged approach using dilatometry and XRD was used to help determine which microstructural changes could be leading to changes in the SS.

3.5 Dilatometry

The simulated heat treatments performed in the Gleeble during LUMet testing were replicated within a Linseis quenching dilatometer. In general, the dilatometry and LUMet data showed the same trends in signal with temperature; however, the dilation and SS changed in opposite directions. Figure 11 shows a representative comparison of the two signals for the 200-300-200 loop. The dilatometry results show a change in dilation at 200 °C after heating to 300 °C and a change in dilation while being held at 300 °C, replicating the LUMet signal and providing reassurance that the LUMet is detecting legitimate microstructural changes. Notably, the dilatometer shows an increase in length (dilation) during the 300 °C hold and ends at a greater length than it started. One possible cause for an increase in length would be decomposition of austenite as the austenite phase is more closely packed than martensite/ferrite.

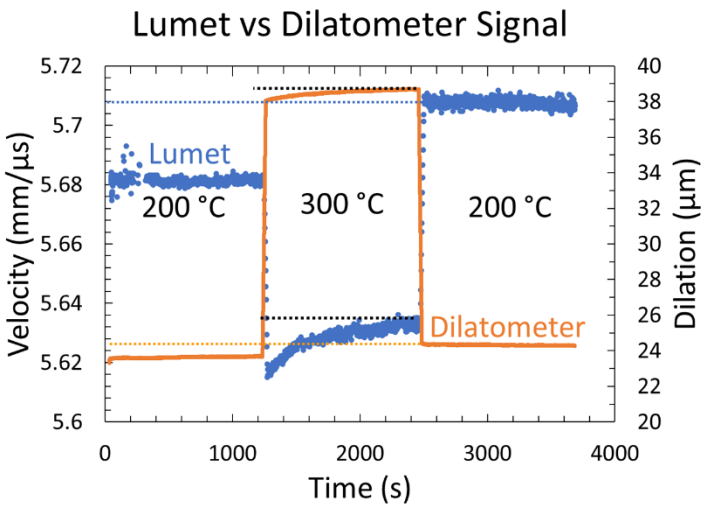

Figure 11. Dilatometry measurements overlayed with LUMet signal.

3.6 XRD Verification

Since it was thought that retained austenite in the sample was influencing some of the changes in the SS, XRD was performed on each condition to look for differences in austenite fraction. Figure 12 shows spectra for the starting powder and the SR sample (prior to heat treatment) with both ferrite/martensite and austenite peaks.

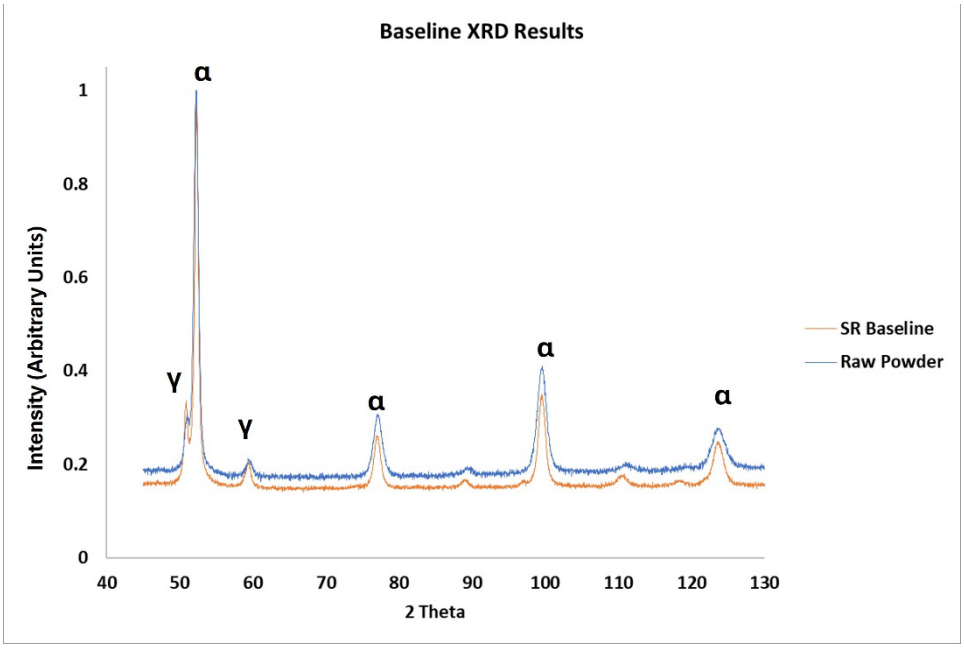

Figure 12. Baseline XRD results showing both ferritic (α) and austenitic (γ) iron are present.

By performing a Rietveld analysis of the XRD data the percentage of retained austenite in each sample was calculated (Table 3). These calculations clearly show that the amount of retained austenite is much lower after the stress relief (19% as-printed vs. 13% in the SR condition).

Table 3. Calculated percentages of retained austenite.

Sample description	SR prior to heat treatment	NSR
As-printed (NSR baseline)	. . .	19.1
SR (SR baseline)	13.3	. . .
0.02 Strain/RT-200-300 loop	13.3/12.3	. . .
0.05 Strain/RT-200-300 loop	9.6/8.6	. . .
0.08 Strain/RT-200-300 loop	7.5/7.6	. . .
200 °C 1 h	10.6	. . .
200–300 °C loop	10.2	. . .
300 °C 1 h	11.5	. . .
RT-200 °C loop	13.8	19.1
RT-200-300 loop	10.6	14.6
RT-300	. . .	14.1
RT-300 four cycles	. . .	15.5
RT-300 five cycles	. . .	15.8

Further consideration of the SR samples shows that continued austenite decomposition occurs with thermal treatments in the 200–300 °C range. While the RT-200 loop shows a similar fraction to the as-SR condition, the 200 °C 1-h condition shows appreciable austenite decomposition. All the 300 °C peak loops show appreciable austenite decomposition. The strained samples both before and after LUMet heat treatments are also interesting to consider. The 0.02 strained sample shows limited decomposition of austenite while nearly half of the austenite has transformed following the application of 0.08 strain. The strain samples also show limited response to subsequent thermal treatment. The RT-200-300 loop did not lead to a significant change in austenite fraction for any of the strained samples. The lack of austenite transformation in the 0.02 strain sample likely indicates that the austenite primarily contributes to the tensile properties via TRansformation Induced Plasticity (TRIP).

The NSR samples have higher fractions of austenite for all LUMet trials as expected. The most interesting point is that the short RT-200 loop again has no effect on austenite fraction and that even the RT-300 loop leaves a higher fraction of austenite than the as-SR condition.

The samples that were heated to 300 °C multiple times show significant changes in retained austenite relative to baseline but not to each other or other samples heated to 300 °C.

A plot of both hardness and the measured retained austenite fraction is shown in Figure 13. There is some correlation that large fractions of retained austenite led to lower hardness in the NSR conditions, though the trend is not clear for the SR samples. The strained SR samples show concurrent increases in hardness with decreased retained austenite as expected.

Figure 13 further demonstrates that hardness is not an ideal criterion for differentiating among conditions for screening purposes. Many of the conditions have hardness within the standard deviation despite significant differences in austenite fraction (recall the significant differences among the tensile properties and hardness discussed earlier).

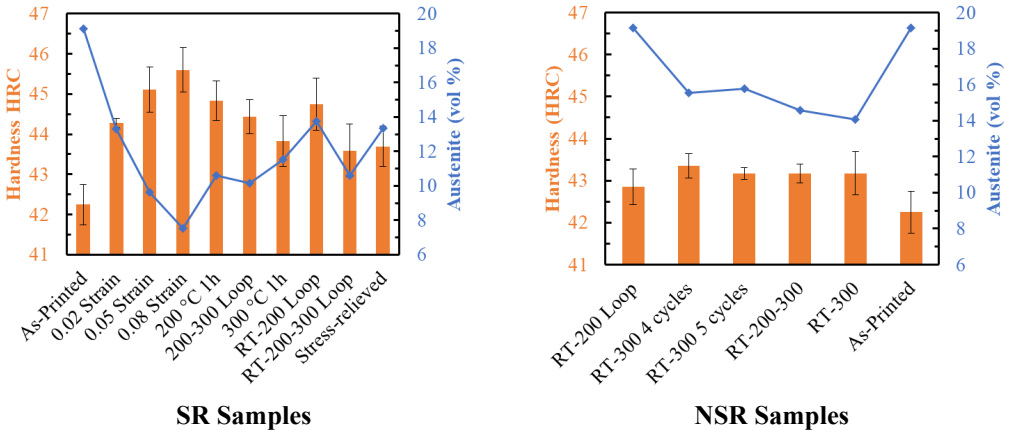

Figure 13. Hardness and retained austenite fraction vs. heat treatment for SR (left) and NSR (right) samples.

3.7 EBSD Results

EBSD was performed to show a semiquantitative visualization of the change in austenite with different strains and thermal treatments (Figure 14). In general, the EBSD results show the same trends in austenite fraction as the XRD results. EBSD does not have the resolution to pick up fine film-like austenite and is sampling a much smaller volume compared with XRD, making the results more qualitative. EBSD results do show a large proportion of blocky austenite, which is thought to be less mechanically stable and less ideal for mechanical properties and toughness. Further study on the austenite fraction/morphology would be of interest but is outside the scope of this work. Overall, while the measured volume percentages between XRD and EBSD do not perfectly match up (due to variabilities in methods and volume sizes used for each technique) they do show the same trends both with regard to heat treatment temperatures and prestrain effects.

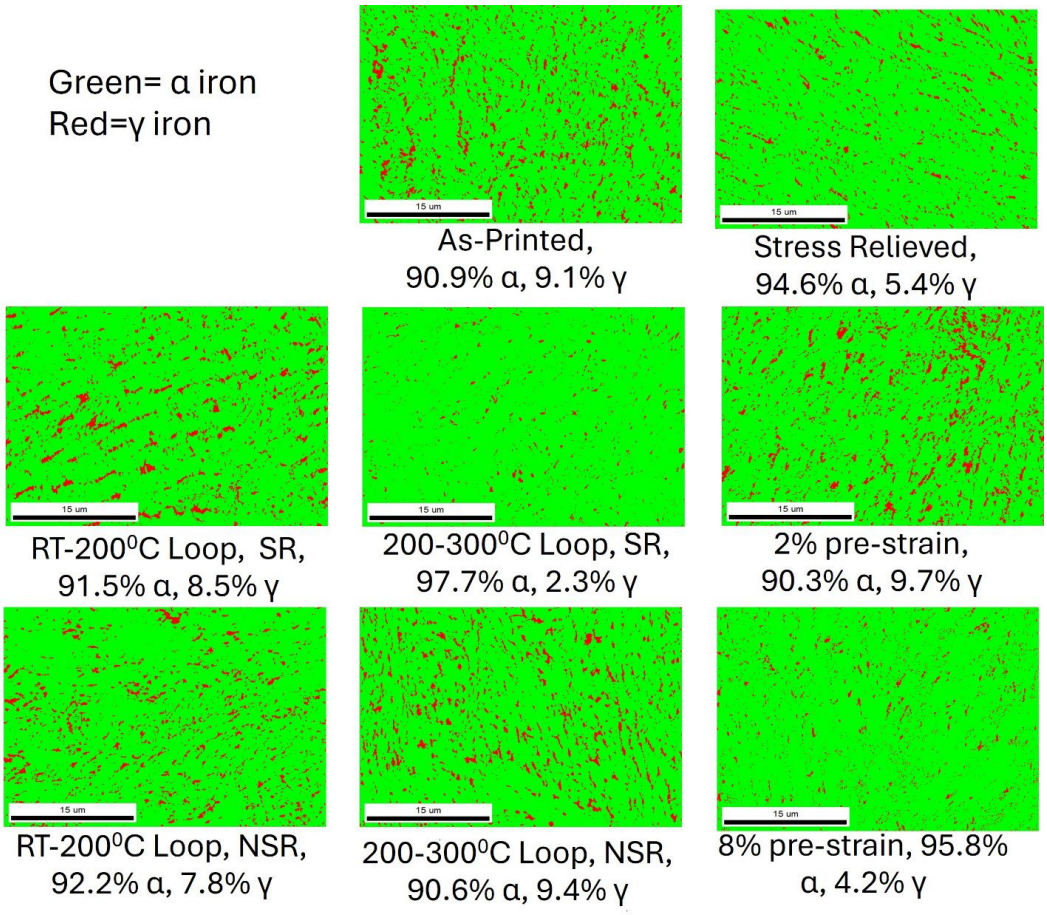

Figure 14. Representative EBSD phase maps of selected LUMet samples.

4. Conclusions

This study began as a series of experiments to determine if the LUMet would prove a reliable method to assess stress relief in AM builds. The efficacy of the LUMet for stress-relief tracking was shown to be limited by the complex microstructures of steel, porosity, and heterogeneity of the AM material. It was demonstrated using XRD and dilatometry that the LUMet could track changes in austenite fraction in the steel. However, the utility of the LUMet for austenite decomposition remains somewhat limited at this state. While with the current setup that was not feasible (a second detection method to pick up transverse waves traveling through the sample may be needed to make these, and other physical property measurements), a method to track the decomposition of austenite during heat treatments and verify that the LUMet could track phase changes in situ was explored. If the starting samples had contained known initial volume percentages of retained austenite, it might have been possible to correlate the magnitude of the signal change after heating to a direct measurement of how much retained austenite transformed to ferrite.

5. References

1. ASTM F3177-21. Standard specification for additive manufacturing—general principles—fundamentals and vocabulary. ASTM International; 2022.

2. Kudzal A et al. Effect of scan pattern on the microstructure and mechanical properties of powder bed fusion additive manufactured 17-4 stainless steel. Mater Des. 2017;133:205–215. https://doi.org/10.1016/j.matdes.2017.07.047

3. Kudzal A, McWilliams B, Taggart-Scarff J, Knezevic M. Fabrication of a low alloy ultra-high strength (>1500 MPa yield) steel using powder bed fusion additive manufacturing. Mater Sci Eng A. 2020;770:138512. https://doi.org/10.1016/j.msea.2019.138512

4. Seede R et al. Effect of heat treatments on the microstructure and mechanical properties of an ultra-high strength martensitic steel fabricated via laser powder bed fusion additive manufacturing. Addit Manuf. 2021;47:102255. https://doi.org/10.1016/j.addma.2021.102255

5. Boyer H, Gall T, editors. Metals handbook desk edition. American Society for Metals; 1992.

6. Khairi MTM et al. Ultrasound computed tomography for material inspection: principles, design and applications. Measurement. 2019;146:490–523. https://doi.org/10.1016/j.measurement.2019.06.053

7. Dubois M, Moreau A, Militzer M, Bussière JF. Laser-ultrasonic monitoring of phase transformations in steels. Scr Mater. 1998;39(6):735–741.

8. Dubois M, Militzer M, Moreau A, Bussière J. A new technique for the quantitative real-time monitoring of austenite grain growth in steel. Scr Mater. 2000;42(9):867–874.

9. Dubois M, Moreau A, Bussière J. Ultrasonic velocity measurements during phase transformations in steels using laser ultrasonics. J Appl Phys. 2001;89(11):6487–6495. https://doi.org/10.1063/1.1363681

10. Lamouche G, Bolognini S, Kruger SE. Influence of steel heat treatment on ultrasonic absorption measured by laser ultrasonics. Mater Sci Eng A. 2004;370(1–2):401–406. https://doi.org/10.1016/j.msea.2003.07.019

11. Moreau A, Kruger S, Côté M, Bocher P. In-situ monitoring of microstructure during thermomechanical simulations using laser-ultrasonics. In: Proceedings of the 1st International Symposium on Laser Ultrasonics: Science, Technology and Applications; 2008 July 16–18; Montreal, Canada.

12. Wang K, Zhao Z. Application of laser-generated ultrasonic to phase transformation analysis in shape memory alloy sheets. Appl Phys Express. 2012;5(1):016601. https://doi.org/10.1143/APEX.5.016601

13. Arguelles A, Turner JA. Ultrasonic attenuation of polycrystalline materials with a distribution of grain sizes. J Acoust Soc Am. 2017;141(6):4347–4355. https://doi.org/10.1121/1.4984290

14. Keyvani M. Laser ultrasonic investigations of recrystallization and grain growth in cubic metals [dissertation]. University of British Columbia; 2018.

15. Rodrigues MM, Militzer M. Laser ultrasonic measurements of phase transformation kinetics in lean Ti–Mo alloys. Metall Mater Trans A. 2022;53(10):3893–3905. https://doi.org/10.1007/s11661-022-06792-1

16. ASTM E8/E8M-16a. Standard test methods for tension testing of metallic materials. ASTM International; 2016.

17. Das A, Chakraborti PC, Tarafder S, Bhadeshia HKDH. Analysis of deformation induced martensitic transformation in stainless steels. Mater Sci Technol. 2011;27(1):141–145. https://doi.org/10.1179/026708310X12668415534008

18. ASTM E23-25. Standard test methods for notched bar impact testing of metallic materials. ASTM International; 2025.

19. Kruger S, Damm E. Monitoring austenite decomposition by ultrasonic velocity. Mater Sci Eng A. 2006;425(1–2):238–243. https://doi.org/10.1016/j.msea.2006.03.056

List of Symbols, Abbreviations, and Acronyms

AM	Additive Manufacturing
CVN	Charpy V-Notch
EBSD	Electron Backscatter Diffraction
LPBF	Laser Powder Bed Fusion
LUMet	Laser Ultrasound Measurement
NSR	Not Stress-Relieved
RT	Room Temperature
SR	Stress-Relieved
SS	Speed of Sound
TRIP	TRansformation Induced Plasticity
UTS	Ultimate Tensile Strength
XRD	X-ray Diffraction

1 (PDF)	DEFENSE TECHNICAL INFORMATION CTR DTIC OCA
1 (PDF)	DEVCOM ARL FCDD RLB CB TECH LIB